Single-Layer Mo_5Te_8 — A New Polymorph of Layered Transition-Metal Chalcogenide

Junqiu Zhang[1§], Yipu Xia[1§], Bo Wang[2], Yuanjun Jin[1,3], Hao Tian[1,3], Wingkin Ho[1], Hu Xu[3], Chuanhong Jin[2], and Maohai Xie[1*]

[1]*Physics Department, the University of Hong Kong, Pokfulam Road, Hong Kong*

[2]*State Key Laboratory of Silicon Materials, School of Materials and Engineering, Zhejiang University, Hangzhou, Zhejiang, 310027, China*

[3]*Department of Physics, Southern University of Science and Technology, Shenzhen, Guangdong, 518055, China*

[§] These authors contributed equally to this work.

* Corresponding author. Email: mhxie@hku.hk

Keywords: polymorphism, transition-metal chalcogenides, two-dimensional materials, MBE, STM

Abstract

Single-layer (SL) transition-metal chalcogenides (TMCs) represent an important family of two-dimensional (2D) materials that have attracted intensive research attention recently. It has been established that many TMCs are polymorphic that can exist in

different crystal structures and correspondingly exhibit diverse physical properties. Discovery of new structural phases of a crystal is of great scientific and practical importance. In this work, we report a new polymorph of SL-TMC, i.e., SL-Mo_5Te_8, attained by molecular-beam epitaxy (MBE). Like the 1*H*-$MoTe_2$, it possesses the hexagonal symmetry but a much larger unit cell with a basis containing as many as 39 atoms (15 Mo and 24 Te). We call it the variational hexagonal (v1*H*) phase. Coincidently, it may be viewed also as one containing the highest density possible of mirror-twin domain boundaries (MTBs) in an otherwise pristine 1*H*-$MoTe_2$. Electronically, it is metallic and a comparison between theory and experiments of its density-of-states (DOS) at the Fermi level reveals features pointing to an importance of electron interactions that invites further investigations.

1. Introduction

Many SL-TMCs with the molecular formula MX_2, where M and X denote the transition-metal (e.g., Mo and W) and chalcogen atoms (e.g., S, Se, and Te) respectively, show polymorphism related to the stacking of the three atomic layers X-M-X. These include the hexagonal (1*H*), octahedral (1*T*) or distorted octahedral (1*T*') phases (see Supplementary Information Figure S1)[1-3]. For some, such as SL-$MoSe_2$ and MoS_2, the 1*H* phase is most stable, which show semiconducting characteristics with direct energy bandgaps[4-6]. For others, such as WTe_2, the metallic 1*T*' phase is more stable and exhibit some interesting properties including huge magnetoresistivity[7] and superconductivity[8]. In certain cases, such as in SL-$MoTe_2$, it is not uncommon to observe both 1*H*, 1*T* and/or 1*T*' phases coexisted in one and the same sample[9, 10]. The ability to tune the phases of a material and thus the properties, e.g., from metallic to insulating, may lead to novel phase-change electronics, and so the discovery and realization of new phases of a material can be of great scientific and practical importance.

Here we report the discovery of a new polymorphic phase of SL-TMC by growth using MBE. Different from all the known phases of SL-MX_2, this new polymorph is chalcogen (Te) deficient having the composition of Mo_5Te_8 and is formed favorably under the less Te-rich conditions of MBE. Due to its hexagonal symmetry and connection with the 1*H* phase, we call it the variational hexagonal phase, or v1*H*, of the SL-TMC.

Deposition of Mo_5Te_8 on bilayer graphene, obtained by heating SiC(0001), or on highly oriented pyrolytic graphite (HOPG) was conducted in a customized MBE reactor from elemental sources. The as-grown films were characterized by angular dark-field scanning transmission electron microscopy (ADF-STEM), low-temperature scanning tunneling microscopy/spectroscopy (STM/S), low-energy electron diffraction (LEED) and ultraviolet photoemission spectroscopy (UPS) for their structural and electronic characteristics (see 'Methods' for details). Similar to previous reports, the 1*H* or 1*T*' phase of $MoTe_2$ is routinely obtained under the Te-rich conditions of MBE, and in certain cases mixture of phases is obtained in one and the same sample (see Supplementary Information Figure S2)[9, 10]. Besides these two common phases, we have observed a new structure, i.e., the v1*H* phase, which forms in large scale under certain conditions. This new structure possesses the hexagonal symmetry and has a basis containing 39 atoms in a unit cell. It belongs to the $P\bar{6}2m$ (No. 79) layer group, a structure that has never been observed previously in any other crystals.

2. Structure of Mo_5Te_8

Figure 1a presents an ADF-STEM image of such a sample revealing the atomic structure of this particular polymorph. From the first sight, it looks like the 1H-phase where atoms are arranged in a hexagonal lattice. However, like in MBE-grown $MoSe_2$, the film is segmented into triangular domains by the MTB defects. Different from the so-called wagon-wheel like arrangement of the MTBs in 1H-$MoSe_2$[11-13], however, the MTBs in epitaxial $MoTe_2$ are super dense, being of the highest density possible. The nano-beam diffraction (NBD) spectrum of the sample is shown in Figure 1b(i). Again, unlike the previously reported “David star” like patterns from the wagon-wheel structure where the diffraction spots are connected by lines[12], here some discrete and sharp spots appear, revealing a highly ordered periodic structure in real space. While the diffraction spots marked by the red circles happen to coincide with that of a pristine 1H-$MoTe_2$, there are many additional spots in between that may only be accounted for by the proposed v1H-Mo_5Te_8 structure (marked by arrowheads). For comparison, a LEED pattern of the sample taken *in situ* immediately after the deposition is shown in Figure 1b(ii), showing a similar spectrum as the NBD. Again, diffraction spots coinciding with pristine 1H-$MoTe_2$ are marked by red circles, while some of those attributed only to the v1H-Mo_5Te_8 structure are marked by arrowheads. It shows a hexagonal symmetry and a well-defined periodicity of ~12.79 Å as sketched in Figure

1c. As seen, it has the unit cell of a rhombus as marked by the black lines, in which there are 15 Mo and 24 Te atoms. The MTB-like segments as described earlier are highlighted in yellow in the figure. This new structure of SL-TMC is found to belong to the $P\bar{6}2m$ (No. 79) layer group which, to the best of our knowledge, has not been suggested to exist or experimentally observed ever in any other 2D crystals. Comparing to 1H-$MoTe_2$, it has a reduced stoichiometry of 1.6 (8:5) for Te, i.e., it has the molecular formula of $MoTe_{1.6}$ or Mo_5Te_8 instead of $MoTe_2$. The Wyckoff positions of Mo and Te atoms are summarized in Table S1.

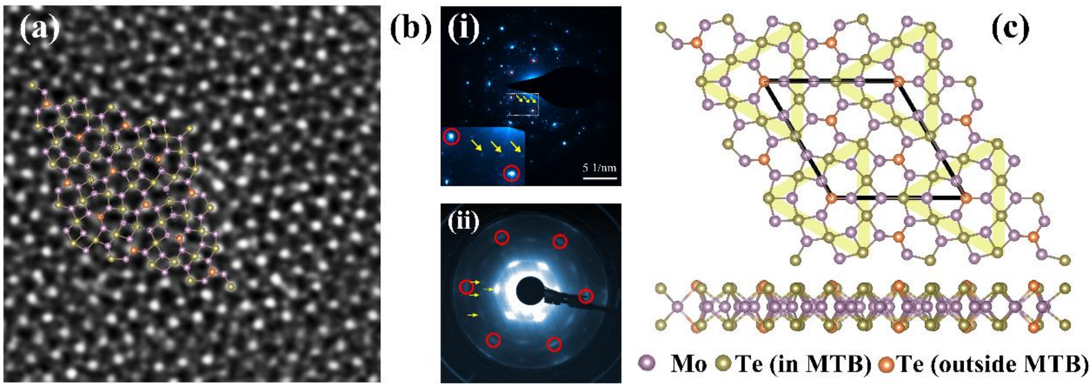

Figure 1. Atomic structure of v1H-Mo_5Te_8. (a) An STEM image of Mo_5Te_8 (size: 6 × 6 nm^2) with a structural model overlaid on part of it. (b) (i) An NBD pattern from a domain of Mo_5Te_8 (size: 377 × 377 nm^2), revealing the symmetry and periodicity of this new structure. The diffraction spots marked by red circles coincide with that of 1H-$MoTe_2$, and that marked by arrowheads are contributed by the v1H-Mo_5Te_8. The inset is an enlargement of selected spots. (ii) A LEED pattern (42.5 eV) of Mo_5Te_8, and as in (i), the red circles mark diffraction spots coinciding with that of 1H-$MoTe_2$. The arrowheads point to some selected diffraction spot attributed solely to v1H-Mo_5Te_8. (c)

Top and side views of the v1*H*-Mo_5Te_8 model, where the black rhombus shown in the top-view marks the unit cell, while the yellow color highlights the MTB segments in the structure. The Te atoms in and outside the MTBs are distinguished by green and orange colors, respectively.

Figures 2a-d present a set of STM images of the same area of a Mo_5Te_8 film but scanned at different sample-to-tip bias conditions. Figures 2a'-d' show simulated STM images at the corresponding biases by the density functional theory (DFT) of the proposed model. The agreement between the experiment and simulation is remarkable, lending a support to the suggested model of v1*H*-Mo_5Te_8. Except that at high negative bias where the image reveals a hexagonal lattice of size ~0.71 nm, corresponding to the distance between the Te atoms outside the MTB segments (marked in orange in Figure 1c), the other images show triangles of different orientations and tiling, where the distance between adjacent triangles is about 1.23 nm. The latter is not far from the DFT calculated lattice constant of a free-standing structure (~ 1.279 nm). The opposite triangles in STM images at different biases correlate respectively to the MTB-loops highlighted in Figure 1c and the 'holes' between the MTB loops.

We note that similar STM images to that of Figure 2 have been previously observed in 1*H*-$MoTe_2$[14] and 1*T*-$TiSe_2$[15, 16], and attributed to charge-density waves (CDW). Particularly in 1*T*-$TiSe_2$, CDW has been well established and known and it is thus tempting to attribute the observation of Figure 2 also to the CDW. On the other hand, a closer look of the results shows not only that the patterns depend on the scanning conditions but also that they have different periodicities. Besides, we do not observe a temperature dependence of the pattern from ~ 5 K to room-temperature. By post-growth treatment of the v1H-Mo_5Te_8 sample in Te environment, we annihilate the v1H-phase (see below) and the patterns as reported in Figure 2 no longer exist. Therefore, we may rule out the patterns to be associated with the CDW in 1H-$MoTe_2$ but assert instead that they stem from the new structure of Mo_5Te_8 as described.

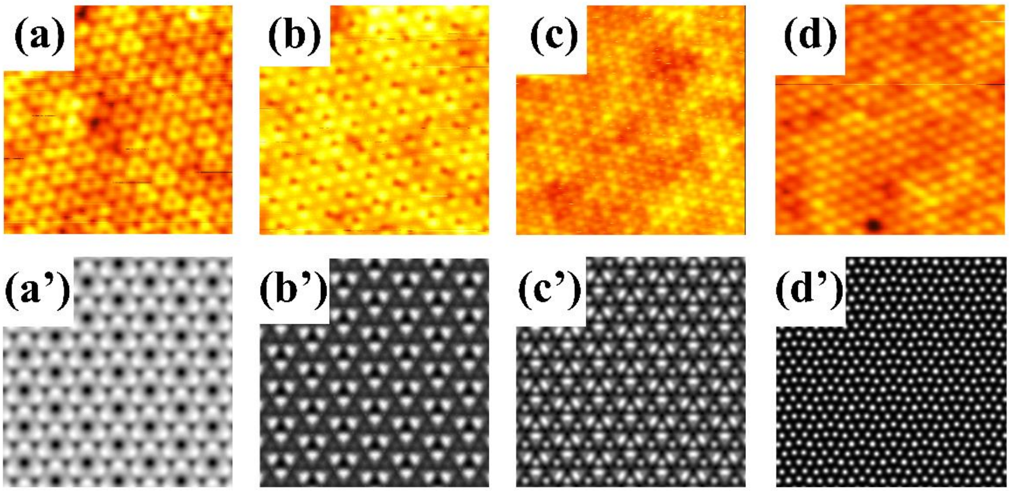

Figure 2. STM images of v1H-Mo_5Te_8. (a-d) STM images (size: 10 × 10 nm^2) taken from Mo_5Te_8 at the sample bias (V_{bias}) of (a) 1.5 V, (b) 0.5 V, (c) -1.0 V, (d) -1.2 V. (a'-d') Simulated STM images (size: 7.7 × 7.7 nm^2) of the v1H-Mo_5Te_8 model by DFT calculations and at energies (a') 1.5 eV, (b') 0.3 eV, (c') -1.0 eV, and (d') -2.0 eV.

3. Stability of Mo_5Te_8

As noted, Mo_5Te_8 has a reduced stoichiometry of 1.6 for Te comparing to 2 in the 1H and 1T' phases of $MoTe_2$. This has in fact reflected the excess of metals in the MTBs in TMCs. It has been reported that formation of a smallest MTB-loop in 1H-$MoTe_2$

would require 3 additional Mo atoms in otherwise a pristine lattice[17]. Expectedly, such a high-Mo or low-Te stoichiometry structure would preferably form at a less Te-rich condition of the MBE, which is supported by our DFT calculations (see below) as well as by experiments. For example, for the v1*H* phase to be consistently obtained and dominant in sample, a relatively low substrate temperature (~ 300℃) and Te/Mo flux ratio (~ 8/1) needs to be carefully controlled. Once grown, it can be stably maintained in vacuum at room temperature for months without apparent degradation or transfer to the other phases of $MoTe_2$. We have in fact also tested the stability of Mo_5Te_8 purposely by taking the sample out of vacuum, keeping it in the ambient condition for 1~2 weeks before being reloaded in vacuum. Follow a gentle annealing procedure (~ 200℃), subsequent LEED/STM measurements recover the result of Mo_5Te_8, suggesting that it is quite stable even in air. On the other hand, annealing the sample at ~ 400℃ with continuous supply of Te will lead to conversion of the v1*H*-Mo_5Te_8 into 1*H*-$MoTe_2$ with the latter still containing MTBs but of lower densities plus some Mo_6Te_6 nanowires[18].

We have conducted some DFT investigations, firstly on the stability of the v1*H*-Mo_5Te_8 phase. Figure 3a presents the calculated formation energy of v1*H*-Mo_5Te_8 as a function of Te chemical potential μ_{Te} and comparing it with that of the 1*H* and 1*T*' phases of $MoTe_2$. The formation energy per atom is defined as

$$E_f(\mu) = \left[E\left(\mathrm{Mo_xTe_y}\right) - x\varepsilon + (2x - y)\mu_{\mathrm{Te}}\right]/(3x)$$

where $E\left(\mathrm{Mo_xTe_y}\right)$ is the system energy of the investigated phase, ε is that of the 1*H* phase per unit cell (i.e., one Mo and two Te atoms) chosen as the energy reference, x and y are respectively the overall composition of Mo and Te atoms in the system. As seen, though the formation energy of v1*H*-Mo_5Te_8 is higher than that of the 1*H* and 1*T*' phases of $MoTe_2$ over the wide range of μ_{Te}, it increasingly approaches that of the 1*T*'-$MoTe_2$ as μ_{Te} decreases, making it more favorable under low Te flux conditions. On the other hand, because of the higher formation energy of Mo_5Te_8 over the whole physically viable range of μ_{Te}, its formation will likely be related to some specific kinetics or the entropy factors or due to an effect of the substrate. Previous reports have shown that a Mo enriched (i.e., Te deficient) environment will favor the 1*T*' phase $MoTe_2$ growth[19, 20]. In a parallel experiment where we chose a higher Te/Mo flux ratio of ~ 15/1 and also at a higher growth temperature (~ 400 °C), instead of v1*H*-Mo_5Te_8, we indeed obtained a film being dominantly 1*T*'-$MoTe_2$ (~ 80% in coverage as estimated by our STM and STEM measurements). Maintaining the same high Te/Mo flux ratio but increasing the substrate temperature further to ~ 500 °C has led to a film dominated by the 1*H*-$MoTe_2$ phase.

In passing, we wish to remark that it is often the case that the as-grown $MoTe_2$ samples contain mixtures of different phases, 1*H*, 1*T*' and the v1*H*, with only the relative weight being sensitively dependent on the MBE conditions. Figure 3b presents an STM image revealing a region containing all three phases manifested in different contrast. We also find that the v1*H*-Mo_5Te_8 domains often join the 1*H*-$MoTe_2$ domains rather than the 1*T*' domains in a sample. The latter may be indicative of a kinetic pathway where Mo_5Te_8 formation is likely connected to the MTBs in 1*H*-$MoTe_2$. We can adjust the growth condition to make the Mo_5Te_8 dominant as indicated by the dominant and bright diffraction spots of Mo_5Te_8 in the LEED (Figure 1b(ii)). In fact, a ratio of ≥90% Mo_5Te_8 domains has been estimated consistently in optimally grown samples (i.e., Te/Mo ~ 8/1, substrate temperature ~ 300°C) according to statistical analysis of the STM data.

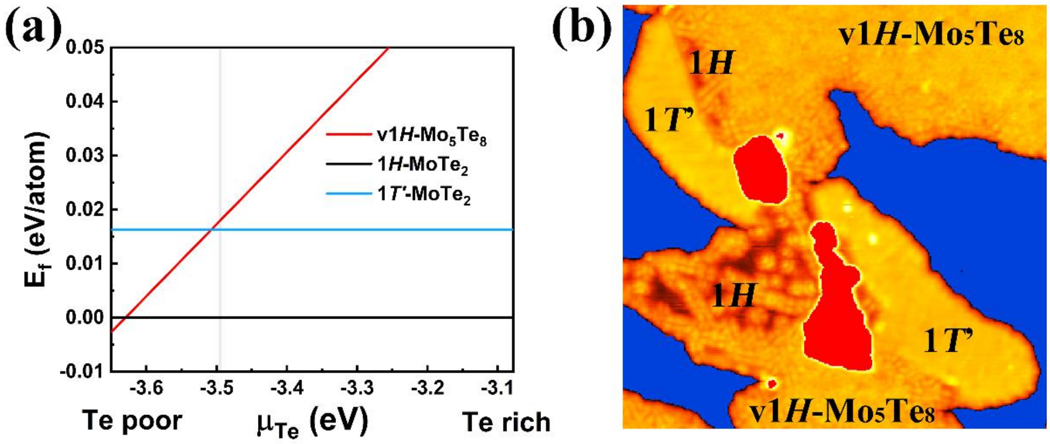

Figure 3. Mo_5Te_8 and phases of $MoTe_2$. (a) DFT calculated formation energy per atom of Mo_5Te_8 and $MoTe_2$. 1*H*-$MoTe_2$, the most stable structure, is set as the energy reference. The range of -3.49 eV < μ_{Te} < -3.08 eV is set by that of bulk Te (μ_{Te}= -3.08 eV) and bulk Mo (μ_{Te}= -3.49 eV), and the lower limit is marked by the vertical grey line. (b) STM image of a sample (size: 50 × 50 nm^2, sample bias: V_{bias} = -1 V) showing a mixture of 1*H*-, 1*T*'-$MoTe_2$, and v1*H*-Mo_5Te_8 domains as marked. The blue background represents graphene substrate, while the middle red-colored regions reflect the 2nd layer of the deposit.

4. Electronic properties

The electronic band of v1*H*-Mo_5Te_8 is also calculated by DFT and the result is shown in Figure 4a. As seen, it has a distinct band structure different from both the semiconducting $1H$- and semi-metallic $1T$'-$MoTe_2$[10]. It reveals a metallic property and the bands near the Fermi level are relatively flat, giving rise to a density-of-states (DOS) peak at $E_F = 0$ eV as shown in Figure 4b. Figure 4c presents typical UPS spectra taken from an as-grown sample *in situ* at different emission angles. These spectra differ from previously reported ones from $MoTe_2$[21, 22], indicating that our sample is indeed of a different structure, i.e., v$1H$-Mo_5Te_8. The prominent peak at around -1.2 eV may correlate well with the high DOS measured by STS (Figure 4d) in the similar energy range. We further note that this photoemission peak is not very dispersive. By comparing with Figure 4a, it appears to correspond well with the nearly flat band at -1 eV. In the UPS spectrum, one further notes a shoulder at the high energy side of the dominant photoemission peak, which may have reflected the dispersive band at -0.69 ~ -0.27 eV. However, due to the limitation of our UPS, we have not been able to verify and separate, studies using high-resolution angle-resolved UPS are called upon in future.

Returning to the DOS of v$1H$-Mo_5Te_8 as presented in Figure 4b, the peak at E_F would make the material unstable with respect to some collective excitations at low temperature. An STS spectrum obtained from such a sample is shown in Figure 4d. We remark that this spectrum is characteristic of v$1H$-Mo_5Te_8, as the same spectrum is obtained irrespective of the very site on v$1H$-Mo_5Te_8 where the measurement is taken. This marks a distinct difference from that of the MTB in $1H$-$MoTe_2$, which shows metallic properties only on the sites of the MTBs but semiconducting in the neighboring $1H$-$MoTe_2$ domains (though for short MTBs, quantum confinement can open DOS gaps[23, 24], see Supplementary Information Figure S2). Figure 4d reveals, besides a metallic behavior different from both 1*H*- and 1*T*'-$MoTe_2$ (see Supplementary Information Figure S2), a DOS suppression at E_F instead of a predicted peak (cf. Figure 4b). The latter may be indicative of some kind of low-energy excitation in system at the temperature of measurement (~ 5 K). On the other hand, we also recognize that v1*H*-Mo_5Te_8 has a higher Mo composition and the energy band is seen narrower than that of 1*T*'-$MoTe_2$, so effects of the Hubbard potential can be also important. We have thus performed the DFT+U calculations and the resulted DOS incorporating a Hubbard potential $U = 2$ eV is shown in Figure 4d (see Supplementary Information Figure S4 for the calculated energy bands). As seen, it reproduces the DOS dip at the Fermi level reasonably well. More studies by experiments and theory are obviously needed to clarify the effect of electron interaction and the true nature of the DOS suppression at E_F, however.

DFT calculations taking into account the spin-orbit coupling in a free-standing SL-Mo_5Te_8 reveal a weak magnetic dipole momentum (see Supplementary Information Figure S5), promising some potentials for magnetic applications. Besides, as the structure of v1*H*-Mo_5Te_8 shows resemblance with MTB-populated 1*H*-$MoTe_2$ and behaves as a metal, it can also be catalytic active that may find applications in catalytic chemistry.

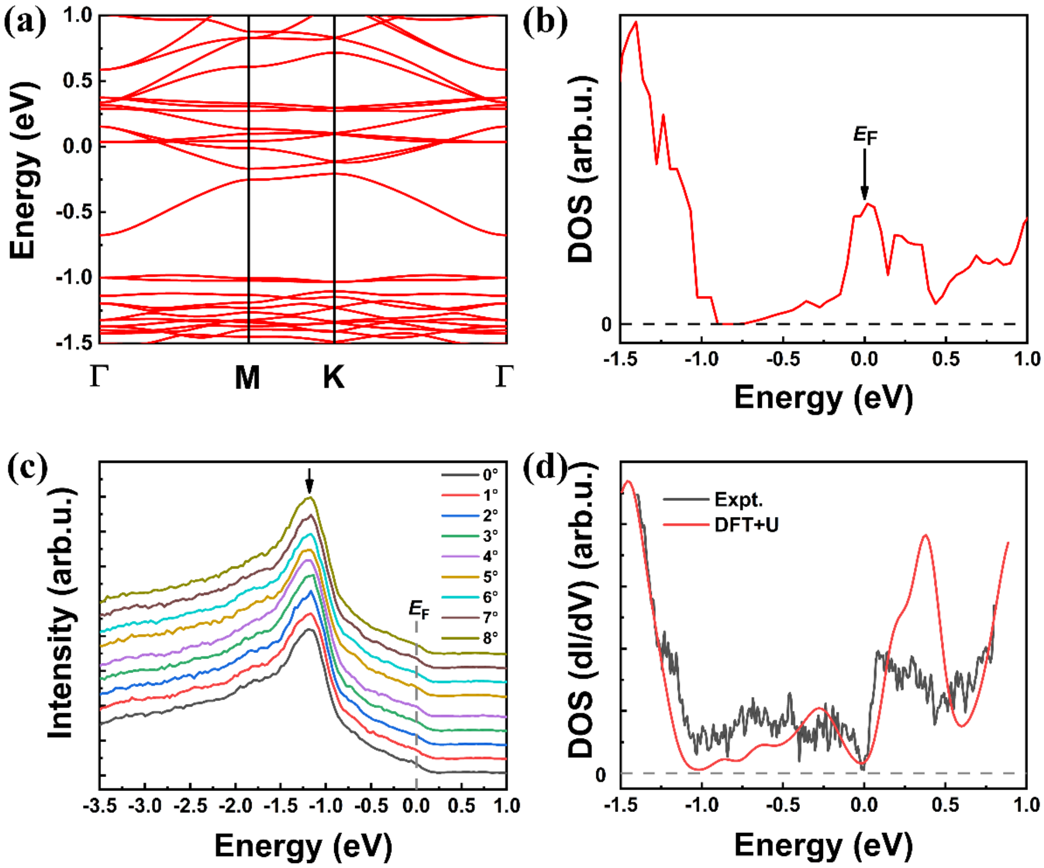

Figure 4. Electronic properties of v1H-Mo_5Te_8. (a) DFT calculated band structure of SL free-standing Mo_5Te_8. (b) DOS of the Mo_5Te_8 as extracted from the DFT-calculated energy bands. Note the high DOS at E_F (0 eV). (c) UPS spectra from a Mo_5Te_8 sample taken from different angles, revealing a major peak at ~ 1.2 eV in binding energy (different spectra are vertically shifted for clarity). (d) STS spectrum taken from Mo_5Te_8 (black curve) and superimposed with the calculated DOS of v1H-Mo_5Te_8 using the DFT+U (U = 2 eV) (red curve, and compare with (b)).

5. Conclusion

To conclude, a new polymorph of SL-TMC, the v1H-Mo_5Te_8, is discovered in films grown by MBE. It has a reduced Te composition (1.6) than the common 1H and 1T'

phases of $MoTe_2$. The structure possesses a hexagonal symmetry and has a unit cell containing a total of 39 atoms (15 Mo and 24 Te). Its structure is closely connected to $1H$-$MoTe_2$ but containing the highest density possible or shortest segments of MTB-loops in an otherwise pristine $1H$-$MoTe_2$. The v$1H$- Mo_5Te_8 is metallic, and the DFT calculations suggest a high DOS at the Fermi energy, whereas STS experiments reveal a DOS suppression at E_F. The latter may be reproduced by a DFT+U calculation (with $U = 2$ eV), indicating possible effect of electron-electron interaction in the system.

6. Methods

SL-Mo_5Te_8 samples were grown on bilayer graphene formed by heating SiC(0001) or on HOPG in an Omicron UHV system with the base pressure of low 10^{-10} Torr. The flux of Mo was generated from an e-beam evaporator and was estimated to be $\sim 1.5 \times 10^{11}$ atoms/cm^2·s. The flux of Te was generated from a standard Knudsen cell operated at 255 °C, which was about 8 times that of Mo during deposition. The substrate temperature was ~300°C.

STM/S measurements of the samples were carried out in a Unisoku 1500 system operated at 77K/5K. The constant-current mode was adopted for all the STM measurements, where the tunneling current was set at 100 pA. As grown samples were either capped by an amorphous Te (or Se) layer or uncapped before being taken out of the vacuum and transferred to the STM system, where a thorough heating procedure is adopted to desorb the capping layer or any adsorbates before the STM/S measurements. Clean surfaces recovered by heating are confirmed by the RHEED and subsequent STM imaging.

ADF-STEM experiments were performed in a probe-corrected STEM (FEI Titan Chemi STEM) operated at 200 kV. The convergence angle was 21.4 mrad and the acceptance angle of the ADF detector was set to 53-200 mrad. This is referred to as the medium angle ADF-STEM (MAADF-STEM) [12, 19]. The specimens for STEM were prepared by the micromechanical exfoliation process and then transferred onto a TEM grid with lacey carbon film. The paraffin wax used during the micromechanical exfoliation were repeatedly washed by acetone, which could substantially decrease possible contamination.

In situ UPS experiments were carried out at room-temperature using a Helium discharge lamp and semi-spherical analyzer. A 3×20 mm^2 slit was inserted in front of the analyzer, which translates into an angle-resolution of ~0.26°.

The DFT calculations were performed by using the Vienna ab initio simulation package (VASP)[25]. The projector augmented wave (PAW) method was applied to describe the interactions between the electrons and core, with the plane-wave cutoff energy 400 eV[26]. We employed Perdew-Burke-Ernzerhof (PBE) formalism of generalized gradient approximation (GGA)[27] to treat exchange-correlation. The k-point sampling of Brillouin zone was set to be $4 \times 4 \times 1$ for the density of states calculations. An effective on-site Coulomb energy $U = 2$ eV is introduced for the DFT+U calculation,

Acknowledgements

We have benefitted from discussions and help from B. Li, S.Y. Gao and J.P. Xu for the UPS experiments. The project is financially supported from a Collaborative Research Fund (C7036-17W) from the Research Grant Council (RGC), Hong Kong Special Administrative Region (HKSAR), a NSFC/RGC joint research grant (No. N_HKU732/17; 51761165024) from the RGC, HKSAR and from the National Natural Science Foundation of China. The authors in ZJU also acknowledged the financial support from the National Natural Science Foundation of China under Grant Nos 51761165024, 51772265, and 61721005, the National Basic Research Program of China under Grant No. 2015CB921004, the Zhejiang Provincial Natural Science Foundation under Grant No. D19E020002, and the 111 project under Grant B16042.The work on electron microscopy was done at the Center of Electron Microscopy of Zhejiang University.

References

[1] Voiry D, Mohite A and Chhowalla M 2015 Phase engineering of transition metal dichalcogenides *Chemical Society Reviews* **44** 2702-12

[2] Chen P, Pai W W, Chan Y H, Sun W L, Xu C Z, Lin D S, Chou M Y, Fedorov A V and Chiang T C 2018 Large quantum-spin-Hall gap in single-layer 1T′ WSe_2 *Nature Communications* **9** 2003

[3] Tang S, Zhang C, Jia C, Ryu H, Hwang C, Hashimoto M, Lu D, Liu Z, Devereaux T P, Shen Z-X and Mo S-K 2018 Electronic structure of monolayer 1T′-$MoTe_2$ grown by molecular beam epitaxy *APL Materials* **6** 026601

[4] Mak K F, Lee C, Hone J, Shan J and Heinz T F 2010 Atomically Thin MoS_2: A New Direct-Gap Semiconductor *Physical Review Letters* **105** 136805

[5] Splendiani A, Sun L, Zhang Y, Li T, Kim J, Chim C-Y, Galli G and Wang F 2010 Emerging Photoluminescence in Monolayer MoS_2 *Nano Letters* **10** 1271-5

[6] Ugeda M M, Bradley A J, Shi S-F, da Jornada F H, Zhang Y, Qiu D Y, Ruan W, Mo S-K, Hussain Z, Shen Z-X, Wang F, Louie S G and Crommie M F 2014 Giant bandgap renormalization and excitonic effects in a monolayer transition metal dichalcogenide semiconductor *Nature Materials* **13** 1091

[7] Ali M N, Xiong J, Flynn S, Tao J, Gibson Q D, Schoop L M, Liang T, Haldolaarachchige N, Hirschberger M, Ong N P and Cava R J 2014 Large, non-saturating magnetoresistance in WTe_2 *Nature* **514** 205
[8] Huang C, Narayan A, Zhang E, Liu Y, Yan X, Wang J, Zhang C, Wang W, Zhou T, Yi C, Liu S, Ling J, Zhang H, Liu R, Sankar R, Chou F, Wang Y, Shi Y, Law K T, Sanvito S, Zhou P, Han Z and Xiu F 2018 Inducing Strong Superconductivity in WTe_2 by a Proximity Effect *ACS Nano* **12** 7185-96
[9] Chen J, Wang G, Tang Y, Tian H, Xu J, Dai X, Xu H, Jia J, Ho W and Xie M 2017 Quantum Effects and Phase Tuning in Epitaxial Hexagonal and Monoclinic $MoTe_2$ Monolayers *ACS Nano* **11** 3282-8
[10] Empante T A, Zhou Y, Klee V, Nguyen A E, Lu I H, Valentin M D, Naghibi Alvillar S A, Preciado E, Berges A J, Merida C S, Gomez M, Bobek S, Isarraraz M, Reed E J and Bartels L 2017 Chemical Vapor Deposition Growth of Few-Layer $MoTe_2$ in the 2H, 1T′, and 1T Phases: Tunable Properties of $MoTe_2$ Films *ACS Nano* **11** 900-5
[11] Liu H, Jiao L, Yang F, Cai Y, Wu X, Ho W, Gao C, Jia J, Wang N, Fan H, Yao W and Xie M 2014 Dense Network of One-Dimensional Midgap Metallic $MoSe_2$ and Their Spatial Undulations *Physical Review Letters* **113** 066105
[12] Hong J, Wang C, Liu H, Ren X, Chen J, Wang G, Jia J, Xie M, Jin C, Ji W, Yuan J and Zhang Z 2017 Inversion Domain Boundary Induced Stacking and Bandstructure Diversity in Bilayer $MoSe_2$ *Nano Letters* **17** 6653-60
[13] Jiao L, Liu H J, Chen J L, Yi Y, Chen W G, Cai Y, Wang J N, Dai X Q, Wang N, Ho W K and Xie M H 2015 Molecular-beam epitaxy of monolayer $MoSe_2$: growth characteristics and domain boundary formation *New Journal of Physics* **17** 053023
[14] Dong L, Wang G-Y, Zhu Z, Zhao C-X, Yang X-Y, Li A-M, Chen J-L, Guan D-D, Li Y-Y, Zheng H, Xie M-H and Jia J-F 2018 Charge Density Wave States in 2H-$MoTe_2$ Revealed by Scanning Tunneling Microscopy *Chinese Physics Letters* **35** 066801
[15] Novello A M, Hildebrand B, Scarfato A, Didiot C, Monney G, Ubaldini A, Berger H, Bowler D R, Aebi P and Renner C 2015 Scanning tunneling microscopy of the charge density wave in 1T-$TiSe_2$ in the presence of single atom defects *Physical Review B* **92** 081101
[16] Spera M, Scarfato A, Pásztor Á, Giannini E, Bowler D R and Renner C 2019 Doping dependent charge density wave contrast inversion in topographic STM images of $TiSe_2$ *arXiv preprint arXiv:1912.02328*
[17] Coelho P M, Komsa H-P, Coy Diaz H, Ma Y, Krasheninnikov A V and Batzill M 2018 Post-Synthesis Modifications of Two-Dimensional $MoSe_2$ or $MoTe_2$ by Incorporation of Excess Metal Atoms into the Crystal Structure *ACS Nano* **12** 3975-84
[18] Xia Y, Wang B, Zhang J, Jin Y, Tian H, Ho W, Xu H, Jin C and Xie M 2020 Quantum Confined Tomonaga–Luttinger Liquid in Mo_6Se_6 Nanowires Converted from an Epitaxial $MoSe_2$ Monolayer *Nano Letters* **20** 2094-9
[19] Cho S, Kim S, Kim J H, Zhao J, Seok J, Keum D H, Baik J, Choe D-H, Chang

K J, Suenaga K, Kim S W, Lee Y H and Yang H 2015 Phase patterning for ohmic homojunction contact in $MoTe_2$ *Science* **349** 625-8

[20] Jana M K, Singh A, Sampath A, Rao C N R and Waghmare U V 2016 Structure and Electron-Transport Properties of Anion-Deficient $MoTe_2$: A Combined Experimental and Theoretical Study *Zeitschrift für anorganische und allgemeine Chemie* **642** 1386-96

[21] Diaz H C, Chaghi R, Ma Y and Batzill M 2015 Molecular beam epitaxy of the van der Waals heterostructure $MoTe_2$ on MoS_2 : phase, thermal, and chemical stability *2D Materials* **2** 044010

[22] Diaz H C, Ma Y, Chaghi R and Batzill M 2016 High density of (pseudo) periodic twin-grain boundaries in molecular beam epitaxy-grown van der Waals heterostructure: $MoTe_2/MoS_2$ *Applied Physics Letters* **108** 191606

[23] Jolie W, Murray C, Weiß P S, Hall J, Portner F, Atodiresei N, Krasheninnikov A V, Busse C, Komsa H-P, Rosch A and Michely T 2019 Tomonaga-Luttinger Liquid in a Box: Electrons Confined within MoS_2 Mirror-Twin Boundaries *Physical Review X* **9** 011055

[24] Xia Y, Zhang J, Jin Y, Ho W, Xu H and Xie M 2020 Charge Density Modulation and the Luttinger Liquid State in $MoSe_2$ Mirror Twin Boundaries *ACS Nano* **14** 10716-22

[25] Kresse G and Furthmüller J 1996 Efficient iterative schemes for ab initio total-energy calculations using a plane-wave basis set *Physical Review B* **54** 11169-86

[26] Blöchl P E 1994 Projector augmented-wave method *Physical Review B* **50** 17953-79

[27] Perdew J P, Burke K and Ernzerhof M 1996 Generalized Gradient Approximation Made Simple *Physical Review Letters* **77** 3865-8